Numerical Simulation of Heat and Mass Transfer in a Continuous Flow Micro-Static Mixer at Different Configurations

Hamdache Abderrazaq*[1], Kiamouche Samir[2], Kernani Redha[1], Drif Seif Eddine[3]

[1] Department of Process Engineering, Faculty of Sciences and Applied Sciences, Bouira University, Drissi Yahia Street, Bouira 10000, Algeria.

[2] Faculty of Process Engineering, University of Constantine 3, Ali Mendjeli, 25000 Constantine, Algeria.

[3] Department of Biochemistry and Microbiology, University of M'sila, M'sila, Algeria.

*****The corresponding author:

E-mail: a.hamdache @univ-bouira.dz

Abstract:

In modern organic chemistry, continuous flow chemistry has been proposed as a means to intensify processes, improve efficiency and control. Laminar flow in the reactor limits micro-mixing to promote reactions and transport phenomena. A thorough understanding of the phenomena is required to understand how the distribution and dispersion of components, heat exchange and pressure drop change based on the geometric configuration. In this work, computational fluid dynamics (CFD) was used to perform a systematic theoretical investigation of the effect of a different design on the performance of passive micro-static mixing.

The finite volume method was used to solve the governing equations. Concentration profiles, temperature, stagnant zones, velocity profiles, and pressure fields are obtained for different designs. The results show that the small square wave static micro-reactor gave the most favorable results.

Keywords: CFD, Continuous flow; Micro-static mixing; Process design.

Nomenclature

Roman Symbols	
CFD	Computational fluid dynamics
x, y	Cartesian coordinates (mm)
U	Horizontal fluid velocity (m/s)
V	Vertical fluid velocity (m/s)
C	Solute concentration (mol/m^3)
C_0	Solute concentration at the upper inlet (mol/m^3)
D	Diffusion coefficient (m^2/s)
Uin	Horizontal fluid velocity at the inlet (m/s)
Vin	Vertical fluid velocity at the inlet (m/s)
Tin	Fluid temperature at the inlet (K)
Tw	Wall temperature (K)
P	Pressure (bar)
Pout	Outlet pressure (bar)
T	Fluid temperature (K)
K	Thermal conductivity W/(m·K)
Greek Symbols	
μ	Fluid viscosity, (Pa/s)
ρ	Fluid density, (g/L)

Introduction

In recent years, there has been an increasing focus on micro-reactors in the chemical and pharmaceutical industries. These reactors are characterized by their tiny internal dimensions, typically on the order of millimeters or even smaller.[1], [2]

Micro-reactors have been proven to offer benefits compared to conventional processing methods when it comes to synthesizing chemical compounds and conducting kinetic studies on a laboratory scale. They are gaining popularity among both academic and industrial researchers who are striving to enhance traditional batch processes.

Over the past twenty years, micro-reactor technology has emerged as a promising method in chemical processing, offering significant advantages over conventional techniques.

These advantages include rapid mixing, increased transport rates, minimized axial dispersion, large specific surface areas, and reduced reactant volumes. However, in certain micro-reactor configurations, achieving the expected conversion is challenging, often due to inadequate mixing of the reactants.[3]– [5]

To improve our understanding of micro-reactors, computational fluid dynamics (CFD) simulations have become increasingly important. This is particularly valuable in understanding the characteristics of flow reactors, which are difficult to assess experimentally. In addition, CFD provides the ability to predict heat transfer and pressure fluctuations.[6]– [8]

Several studies have been carried out to numerically study the chemical reaction efficiency of the microreactors, C. Fernández-Maza et al. [9] performed an experimental and numerical analysis to evaluate the performance of continuous flow microreactors with different curved geometries. T. Frey et al. in 2021 [10] performed a computational fluid dynamics (CFD) investigation to study asymmetric mixing at different inlet configurations within a split-and-recombine micromixer.

M. J. Nieves-Remacha, et al [11] used the OpenFOAM computational fluid dynamics simulator to study single-phase flows in an advanced flow reactor. The results showed strong agreement with experimental pressure drop results.

In 2011 E. V. Rebrov, et al. [12] employed multiple micro-reactor instances to enhance performance through the development of particular designs that consider the best flow and temperature distributions.

The study of Fernández-Maza et al. [13] evaluated the performance of different micro-reactor geometries. The spiral micro-reactor showed the best performance, reducing the reaction time by half. The simulated results were confirmed by experimental analysis, with less than 10% error.

The current study focuses on using computational fluid dynamics to analyze the performance of different configurations on mixing. Diverse designs are investigated to comprehend their flow behavior and heat transfer under laminar conditions.

Problem definition

The selection of geometric configuration has a significant impact on the results obtained. In this particular study, a comprehensive exploration involved the testing of six distinct geometries. These variations in geometric design were examined to assess their individual influences on the results obtained within the study.[14]–[17]

The optimal geometry aims to achieve several key objectives, achieving the most effective temperature homogenization, minimizing pressure drop, and facilitating superior mixing characteristics. This geometry design strives to strike a balance among these factors, ensuring an efficient, uniform temperature distribution, minimal resistance to flow (low pressure drop), and enhanced mixing efficiency within the micro-reactor system.[18]–[21]

Geometrical configuration

In this study, the performance of six different micro-reactor geometries was investigated. These geometries, shown in Figure 1, have two inlets, the upper one (Inlet A) for the concentrated solution and the lower one (Inlet B) for the dilution solution.

The linear channel (Figure 1.A) shows the simplest geometry, (Figure 1.B and C) represents a square wave configuration with a different wavelength. More complex configurations are shown in Figure 1.D, E and F. All of them were designed in FreeCad. The distance measurements provided in the Figure 1 are given in millimeters.

The detailed dimensions of the micro-reactor, precisely depicted in Figure 1, include specific measurements. The length of the micro-reactor measures around 100 mm, while the channel thickness is noted to be 3 mm.

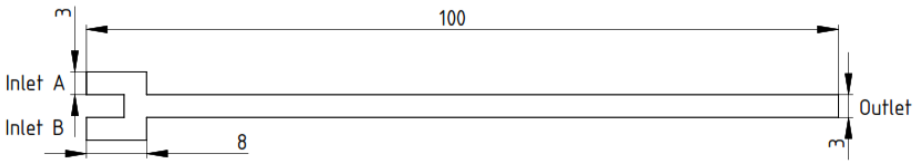

A: straight reactor

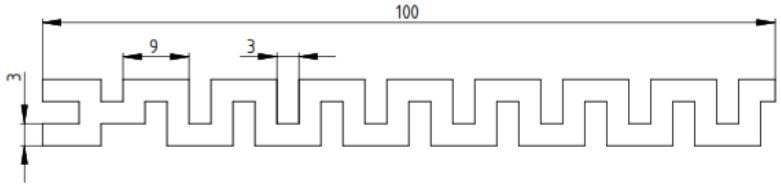

B: larg square wavy

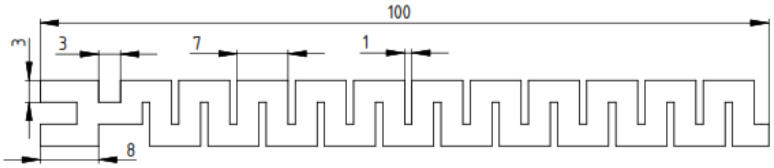

C: small square wavy

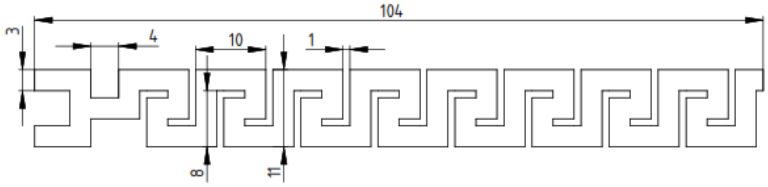

D: serpentine

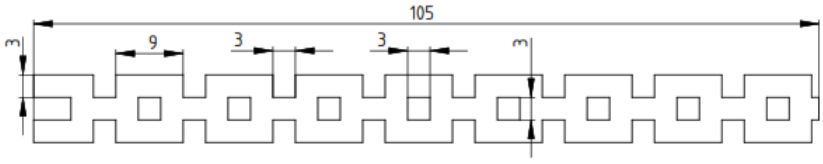

E: larg distanc rectangle

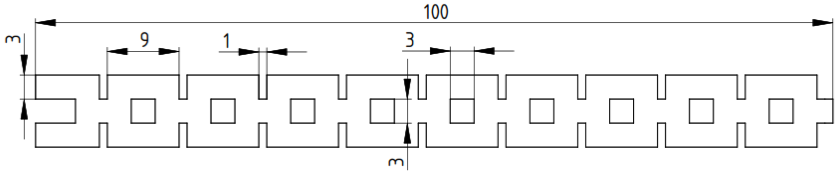

F: small distanc rectangle

Figure 1: Design of the different micro-reactor geometries

Mathematical model

1.1 Physical properties and operating conditions

All pertinent physical properties and operating parameters are summarized in **Table 1**, detailing key symbols, respective values, and their corresponding units:

Table 1: Physical properties and operating conditions.

	Symbol	Value	Unit
Velocity	U_{in}	0.02	m/s
Upper inlet concentration	C_0	1	mol/m^3
Inlet temperature	T_{in}	293.15	K
Wall temperature	$\mathbf{T_{wall}}$	**400**	**K**
Outlet pressure	**Pout**	**0**	**pa**

1.2 Governing equations

The flow is described by the Navier–Stokes equations. Considering the above assumptions, the two-dimensional continuity, mass, momentum and energy equations for an incompressible Newtonian fluid flow are written as follows:[22], [23]

$$\frac{\partial(\rho U)}{\partial x} + \frac{\partial(\rho V)}{\partial y} = 0 \qquad \text{Equation 1}$$

The convection-diffusion mass transfer equation is expressed by Equation 2.

$$\frac{\partial C}{\partial t} + U\frac{\partial C}{\partial x} + V\frac{\partial C}{\partial y} = \frac{\partial}{\partial x}\left(D\frac{\partial C}{\partial x}\right) + \frac{\partial}{\partial y}\left(D\frac{\partial C}{\partial y}\right) \qquad \text{Equation 2}$$

In the case of an incompressible laminar flow. The momentum conservation in the x-direction and y-direction are respectively described by Equation 3 and Equation 4.

$$\rho U\frac{\partial U}{\partial x} + \rho V\frac{\partial U}{\partial y} = \frac{\partial}{\partial x}\left(\mu\frac{\partial U}{\partial x}\right) + \frac{\partial}{\partial y}\left(\mu\frac{\partial U}{\partial y}\right) - \frac{\partial P}{\partial x} \qquad \text{Equation 3}$$

$$\rho U\frac{\partial V}{\partial x} + \rho V\frac{\partial V}{\partial y} = \frac{\partial}{\partial x}\left(\mu\frac{\partial V}{\partial x}\right) + \frac{\partial}{\partial y}\left(\mu\frac{\partial V}{\partial y}\right) - \frac{\partial P}{\partial y} \qquad \text{Equation 4}$$

The conservation of thermal energy can be written as

$$\frac{\partial T}{\partial t} + U\frac{\partial T}{\partial x} + V\frac{\partial T}{\partial y} = \frac{\partial}{\partial x}\left(K\frac{\partial T}{\partial x}\right) + \frac{\partial}{\partial y}\left(K\frac{\partial T}{\partial y}\right) \quad \text{Equation 5}$$

Where x and y are Cartesian coordinates, U and V are the velocity components, P is the pressure, C is the concentration, and T is the temperature of the fluid.

1.3 Boundary conditions

According to researchers, the solute concentration may be constant at the upper inlet. In the present study, the normal velocity, temperature and solute concentration are assumed to be uniform and constant. The tangential velocity Vin is assumed to be negligible. At the lower inlet, the concentration is set to zero.[9], [23], [24]

1.3.1 Upper inlet boundary conditions

$U = U_{in}$, $V = V_{in} = 0$, $C = C_0$, $T = T_{in}$

1.3.2 Lower inlet boundary conditions

$U = U_{in}$, $V = V_{in} = 0$, $C = 0$, $T = T_{in}$

1.3.3 Outlet boundary conditions

At the reactor outlet, the pressure is specified and the tangential derivatives of the velocity, temperature and concentration are set to zero (established flow).

$\frac{dU}{dx} = 0$, $\frac{dV}{dx} = 0$, $\frac{dC}{dx} = 0$, $\frac{dT}{dx} = 0$, P = Pout

1.3.4 Boundary conditions at the channel wall

The non-slip condition is used for the velocities, and the normal gradient of the concentration is zero. The temperature is kept constant (T_{wall}).

$U = 0$, $V = 0$, $n\nabla C = 0$, $T = T_{wall}$

1.4 Numerical methodology

Transport with appropriate boundary conditions is discretized using the finite volume method, and pressure-velocity coupling is handled by the SIMPLER algorithm. Convective terms are discretized using the power law scheme. The resulting algebraic equations are solved using the BiCGStab method. The code is developed in Python 3 with Numpy, Scipy, Pandas and Matplotlib, using the open VS code editor.

Results and discussion

In this section, we examined how different geometries affect various parameters, including concentration, pressure, flow rate, and temperature. During our study, we examined the pressure drop across different geometries and evaluated mixing efficiency and heat transfer to optimize the design of our static micro-mixer.

The results were visualized in 2D for all the parameters, In particular, we plotted concentration and pressure profiles along the channel, precisely 0.5 mm away from the channel wall (indicated by the dotted line in Figure 2). While the temperature profiles were depicted at the mi-distance between the walls (shown by the dashed line in Figure 2).

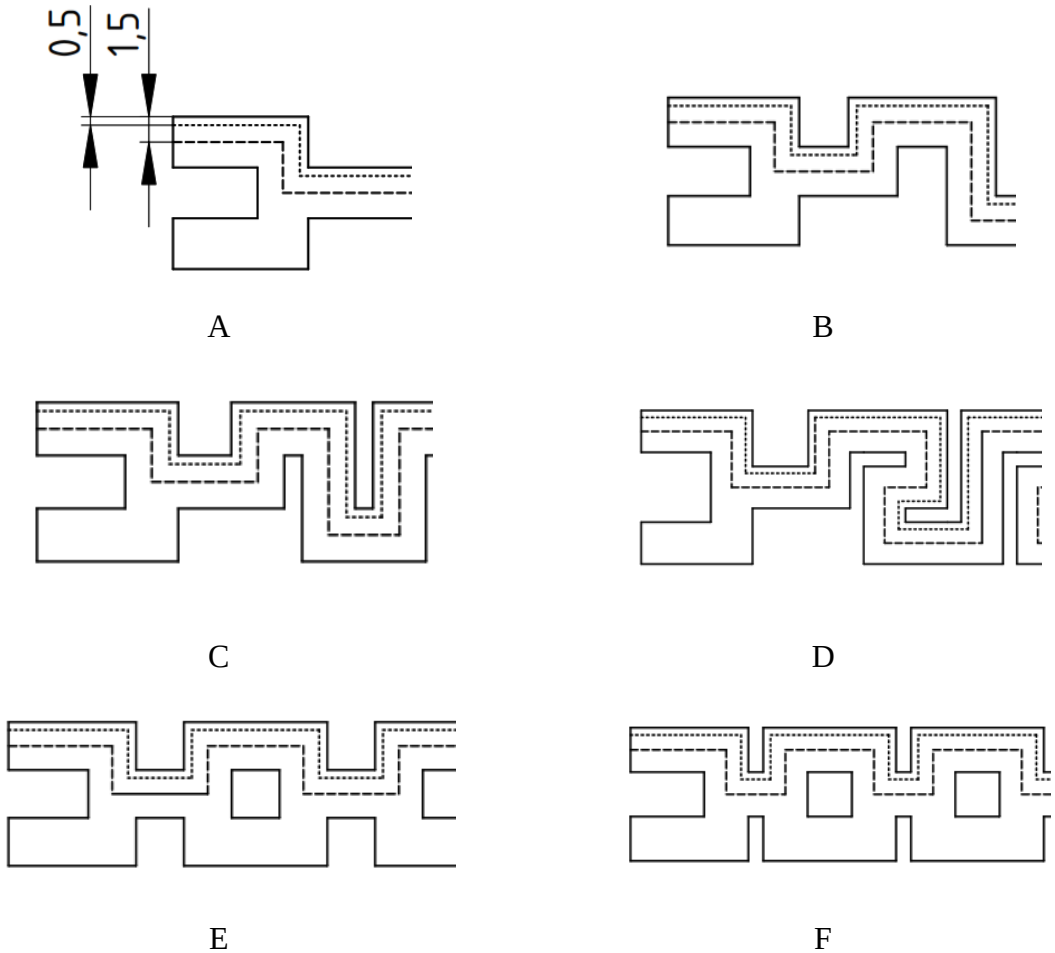

Figure 2: Profile lines across various geometries

1.5 The effect of the geometric configuration on the mixing process

The concentration evolution depicted in Figure 3 highlights the significant influence of the mixer's geometric design on the uniform distribution of chemical species throughout the channel. Our observations indicate that the straight (Figure 3 A), serpentine, and rectangular

configurations (Figure 3 D, E, and F) do not guarantee efficient mixing. Conversely, the square wave geometries (Figure 3 B and C) exhibit superior mixing capabilities.

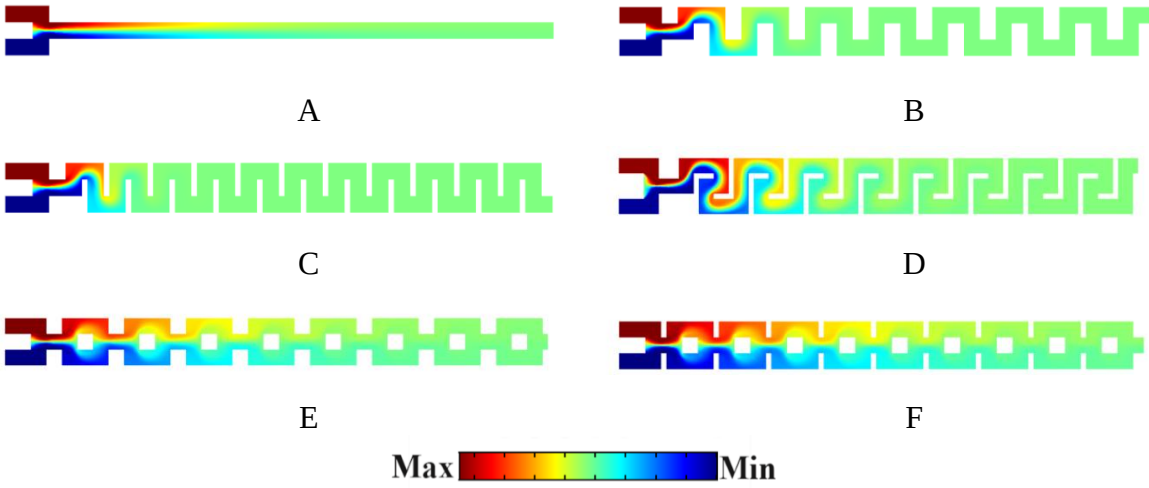

Figure 3: Concentration profiles for the different geometric configurations.

Based on the concentration profile calculated along the channel at a distance of 0.5 mm from the wall (Figure 4) for each reactor configuration distinctly indicates that configurations B and C exhibit superior performance compared to the other reactor geometry.

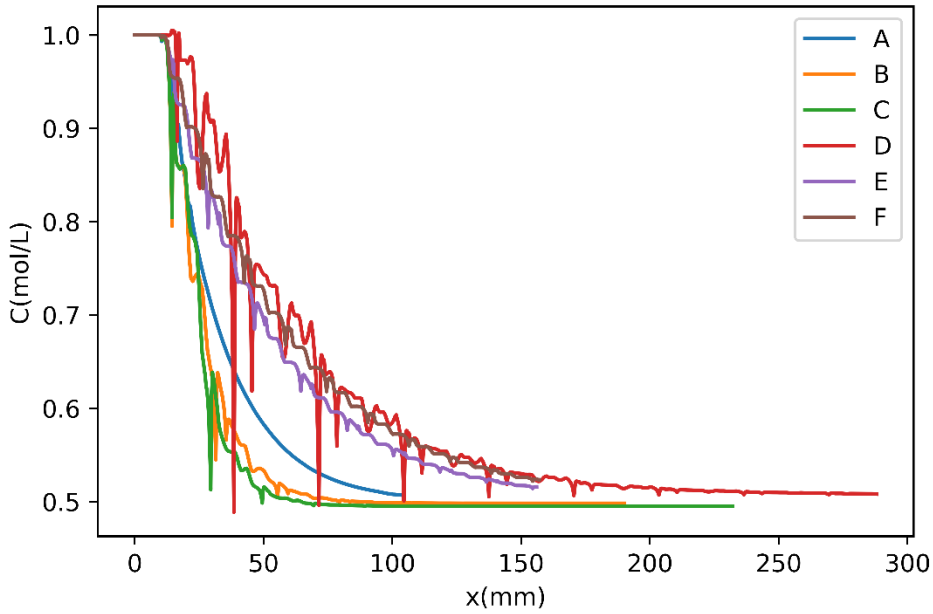

Figure 4: Concentration profiles along the channel at a distance of 0.5 mm from the wall.

1.6 The effect of the geometric configuration on the pressure drop

The influence of geometrical configuration on the pressure drop has been extensively studied in various reactor configurations, revealing that pressure drop varies with alterations in geometry. The pressure drop was found to be elevated for C and D configurations, moderate for B, E, and F configurations, and minimal for A configuration as demonstrated in Figure 5 and Figure 6.

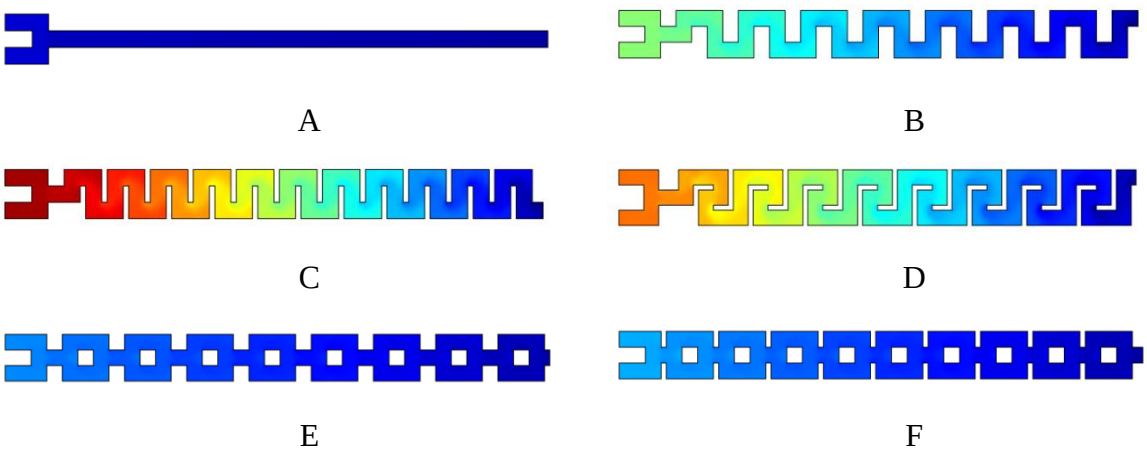

Figure 5: Pressure profiles for the different geometric configurations.

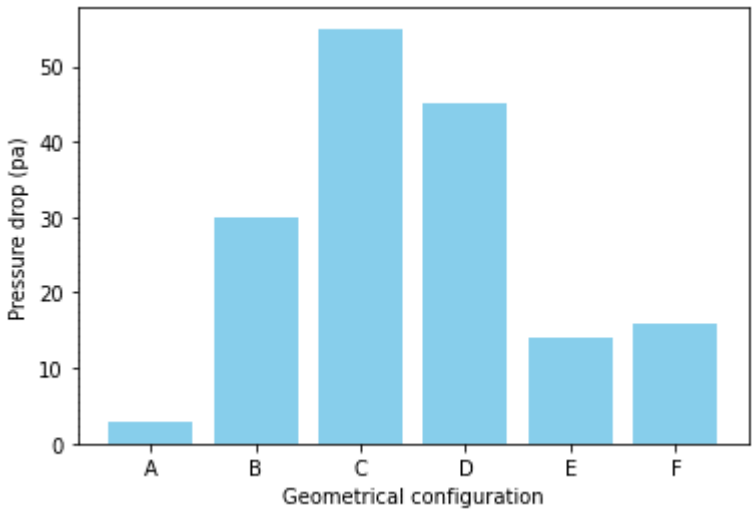

Figure 6: Pressure drop across the entire reactor

As depicted in **Figure 7**, the pressure profiles along the micro-reactors exhibit a nearly linear trend at a proximity of 0.5 mm from the boundary, across all geometric configurations.

The pressure drop increases with the length of the path travelled by the reaction mixture in each micro-reactor, with the exception of reactor C, which has a very steep profile when compared with the others.

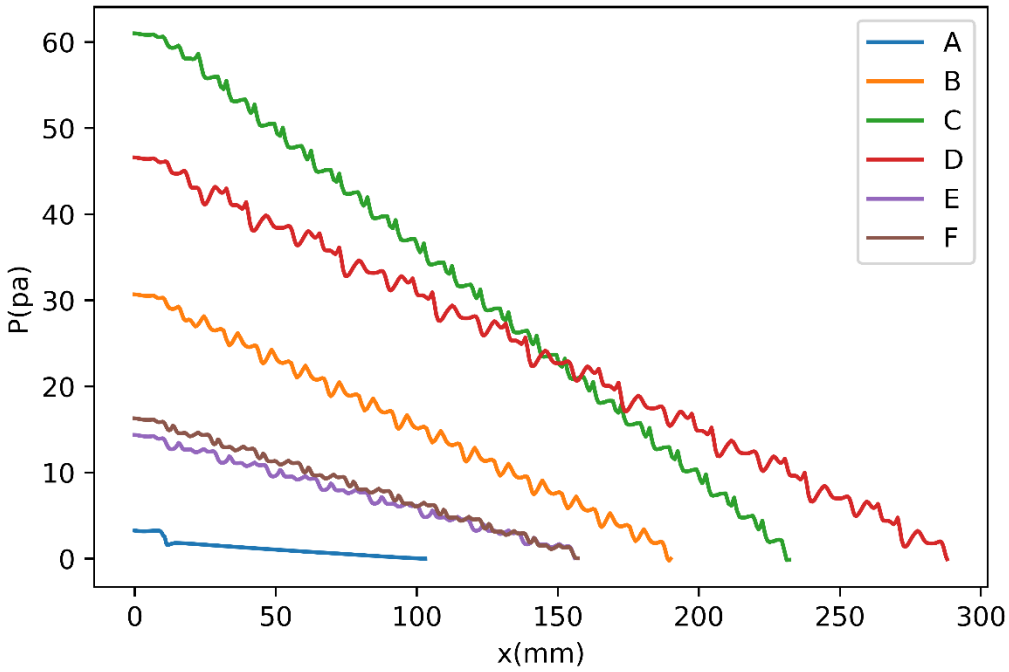

Figure 7: Pressure profiles along the channel at a distance of 0.5 mm from the wall.

1.7 Effect of geometric configuration on temperature homogenization.

In order to raise the temperature of the reaction mixtures, which initially entered at 293.15K, to an ideal temperature for the reaction, we maintained the temperature of the micro-reactor walls at 400K. After running the simulation, it was observed that configuration A had the worst heat transfer performance. Conversely, configuration D gave average results. The other configurations B, C, E and F give good heat transfer performance.

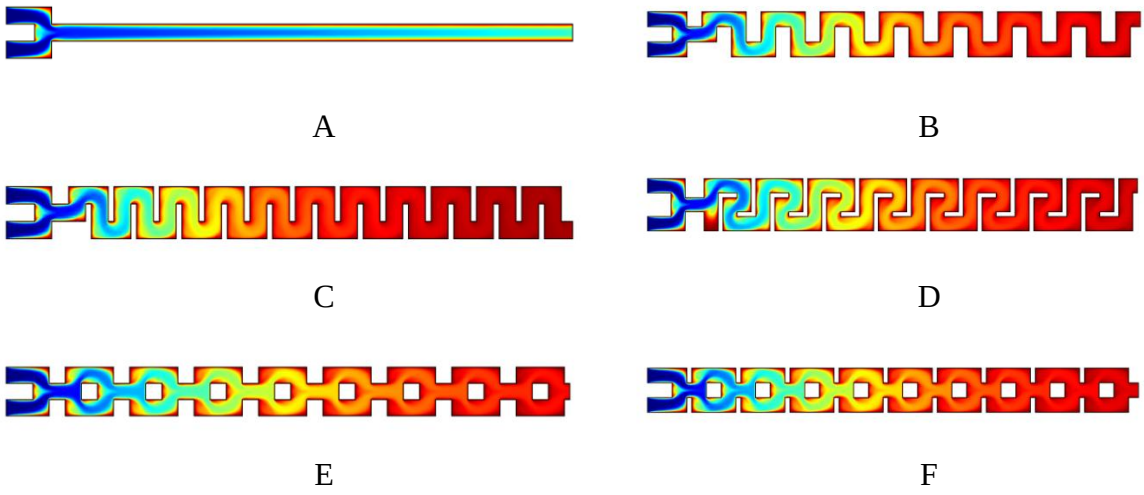

Figure 8: Temperature profiles for the different geometry configurations.

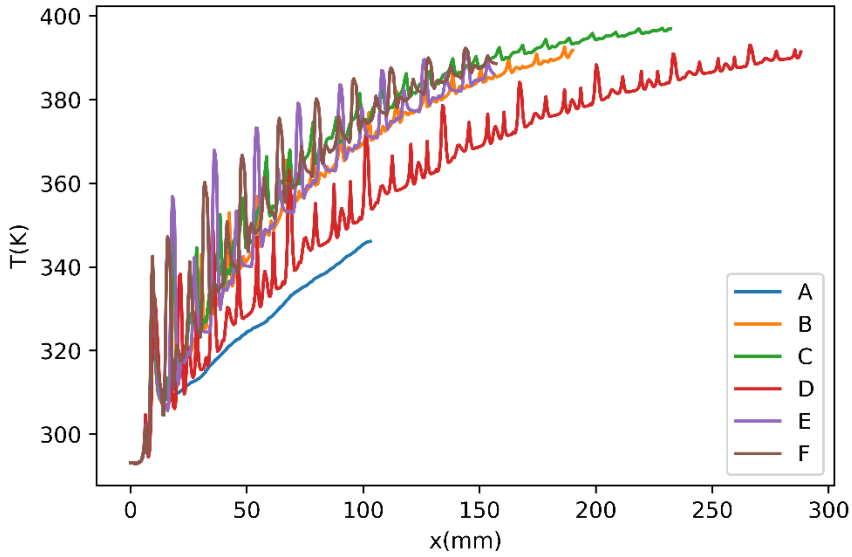

Figure 9: Temperature profiles along micro-reactor at midwall distance.

1.8 Velocity magnitude

We conducted this particular aspect of the study in order to provide a comprehensive and thorough explanation for the aforementioned results that have been cited previously.

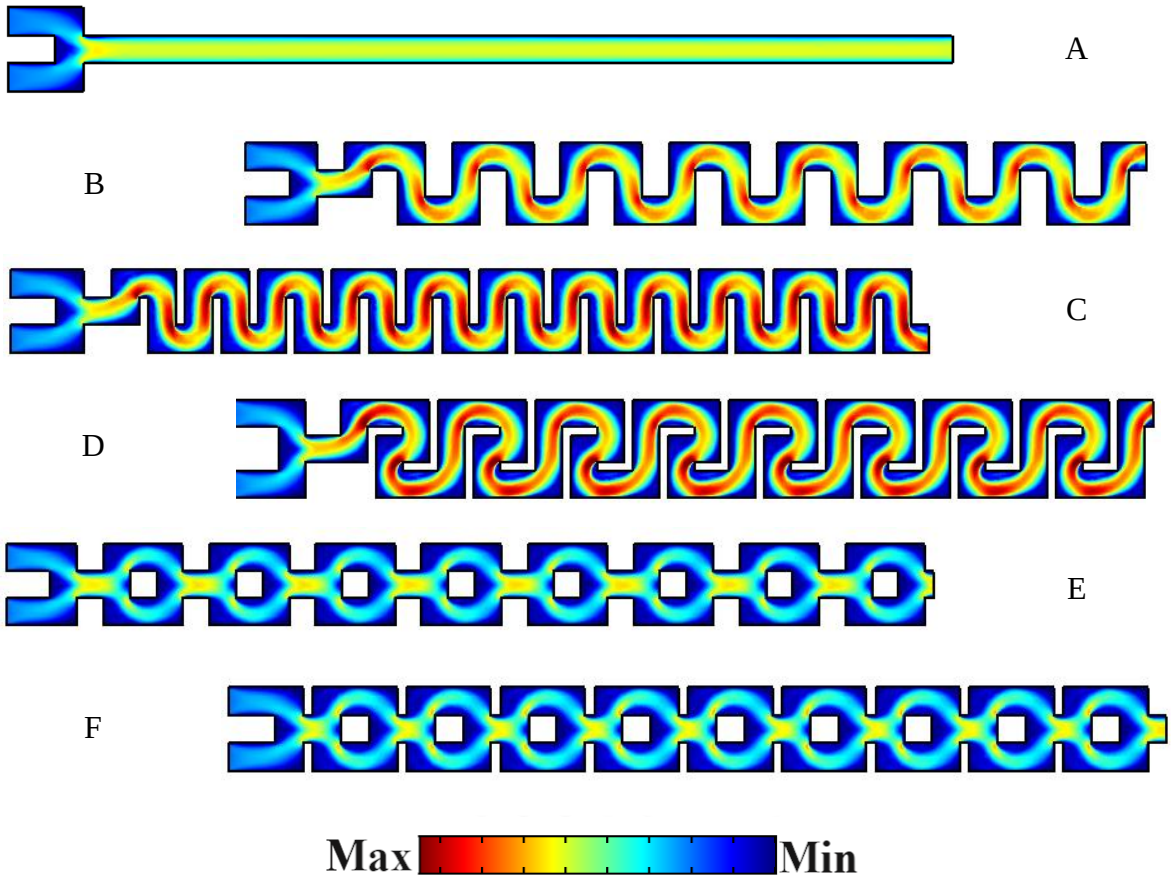

Figure 10: Velocity magnitude profiles for the different geometric configurations.

The comprehension of the velocity profiles associated with each geometric configuration allows for the elucidation of the evolution of the concentration, pressure, and temperature profiles. **Figure 10** shows the velocity profiles for all the geometric configurations, where it can be seen that configurations B, C, and D exhibit significantly increased velocity. This observation explains the significant pressure drop found in these specific configurations.

Configurations B and C ensure good mixing and heat transfer, despite their high pressure drop. We can clearly see (**Figure 11**) in the straight geometry (A) that the velocity practically follows a single direction (x), except at the channel entrance, creating a very thick boundary layer near the walls along the channel. This explains the poor mixing and heat exchange between the micro-reactor walls and the reaction mixture.

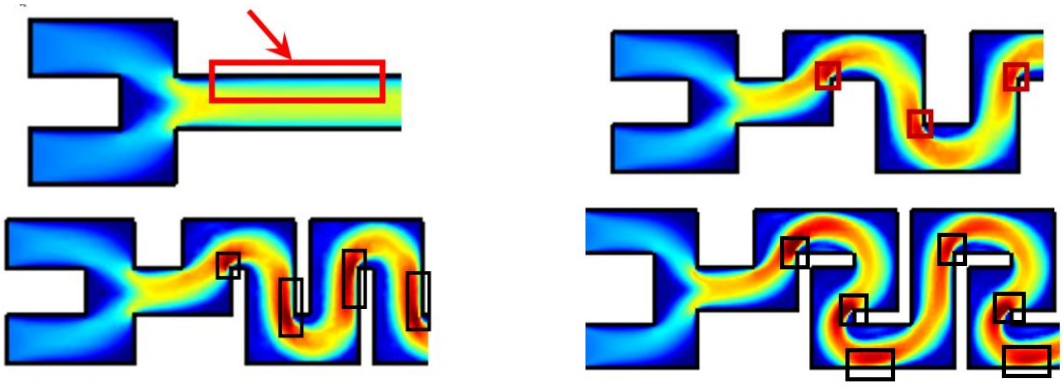

Figure 11: Boundary layer for multiple geometric configurations**.**

The relationship between the size of the high-velocity region and the boundary layer is such that when the high-velocity region is larger, the boundary layer becomes smaller. Additionally, when the high-velocity region increases in size, the process of homogenization also intensifies. This means that as the high-velocity region expands, the boundary layer, which is the layer immediately adjacent to the high-velocity region, decreases in size. Simultaneously, the homogenization process, which refers to the mixing and blending of different substances or elements, becomes more pronounced and effective. Therefore, there exists a direct correlation between the size of the high-velocity region and both the boundary layer and the homogenization process.

Configurations E and F effectively divide the flows into two separate streams (**Figure 12**), thereby reducing the amount of interaction between these two streams. As a result of this flow division, the mixing of the two streams is compromised, resulting in suboptimal homogeneity.

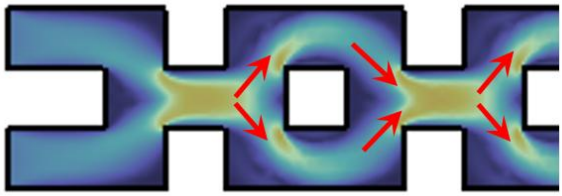

Figure 12: Flow division in geometric configuration E.

The D configuration is considered suboptimal for mixing substances due to its large dead zones (**Figure 13**), which are areas where mixing is less effective compared to other shapes.

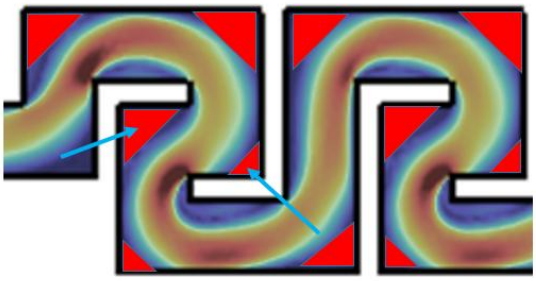

Figure 13: Stagnant zones in D configuration.

Configurations D, E, and F don't ensure good mixing, and configuration A has very low heat transfer, so the remaining configurations are B and C or the square wave configuration (**Table 2**). In conclusion, the wave shape is the most efficient, and the smaller the wave, the higher the efficiency, with an increase in pressure drop.

Table 2: Mixing and heat exchange efficiency for various geometric configurations.

A	Average mixing	Poor heat exchange
B	Good mixing	Good heat exchange
C	Good mixing	Good heat exchange
D	Poor mixing	Average heat exchange
E	Poor mixing	Good heat exchange
F	Poor mixing	Good heat exchange

Conclusion

A detailed holistic study of the mixing performance in different micro device geometries has been carried out using numerical simulation techniques. The main objective of this work is to understand the phenomena that govern the fluid dynamics in different geometric configurations to allow the design of static micromixers. The best performance was obtained with the small square wave micro-reactor, which improved the mixing and heat exchange compared to the large square wave.

The reason for the significant improvement in performance of these geometries is that they have the highest velocity in close proximity to the micro-reactor wall. In addition, these geometries have the smallest dead zone of all the geometries studied. The straight reactor has poor heat exchange and average mixing efficiency. The serpentine, large distance rectangle, and small distance rectangle have poor mixing efficiency.

Declarations

Conflict of interest: All authors certify that they have no affiliations with or involvement in any organization or entity with any financial interest or non-financial interest in the subject matter or materials discussed in this manuscript.

References

[1] H. An, A. Li, A. P. Sasmito, J. C. Kurnia, S. V. Jangam, et A. S. Mujumdar, « Computational fluid dynamics (CFD) analysis of micro-reactor performance: Effect of various configurations », *Chem. Eng. Sci.*, vol. 75, p. 85-95, 2012.

[2] P. Bianchi, J. D. Williams, et C. O. Kappe, « Oscillatory flow reactors for synthetic chemistry applications », *J. Flow Chem.*, vol. 10, p. 475-490, 2020.

[3] S. Bettermann, F. Kandelhard, H.-U. Moritz, et W. Pauer, « Digital and lean development method for 3D-printed reactors based on CAD modeling and CFD simulation », *Chem. Eng. Res. Des.*, vol. 152, p. 71-84, 2019.

[4] H. Calis, J. Nijenhuis, B. Paikert, F. Dautzenberg, et C. Van Den Bleek, « CFD modelling and experimental validation of pressure drop and flow profile in a novel structured catalytic reactor packing », *Chem. Eng. Sci.*, vol. 56, nº 4, p. 1713-1720, 2001.

[5] R. O. Fox, « CFD models for analysis and design of chemical reactors », *Adv. Chem. Eng.*, vol. 31, p. 231-305, 2006.

[6] Y. Cao, N. Padoin, C. Soares, et T. Noël, « On the performance of liquid-liquid Taylor flow electrochemistry in a microreactor – A CFD study », *Chem. Eng. J.*, vol. 427, nº July 2021, 2022, doi: 10.1016/j.cej.2021.131443.

[7] W. Han et X. Chen, « A novel design of nanochannel structure in a micro–nanofluidic preconcentrator for electrokinetic ion enrichment », *J. Braz. Soc. Mech. Sci. Eng.*, vol. 42, nº 1, p. 49, 2020.
[8] N. Yazdanpanah, C. N. Cruz, et T. F. O'Connor, « Multiscale modeling of a tubular reactor for flow chemistry and continuous manufacturing », *Comput. Chem. Eng.*, vol. 129, p. 106510, 2019, doi: 10.1016/j.compchemeng.2019.06.035.
[9] C. Fernández-Maza, M. Fallanza, L. Gómez-Coma, et I. Ortiz, « Performance of continuous-flow micro-reactors with curved geometries. Experimental and numerical analysis », *Chem. Eng. J.*, vol. 437, nº January, 2022, doi: 10.1016/j.cej.2022.135192.
[10] T. Frey *et al.*, « CFD analysis of asymmetric mixing at different inlet configurations of a split-and-recombine micro mixer », *J. Flow Chem.*, vol. 11, nº 3, p. 599-609, 2021, doi: 10.1007/s41981-021-00178-x.
[11] M. J. Nieves-Remacha, A. A. Kulkarni, et K. F. Jensen, « OpenFOAM Computational Fluid Dynamic Simulations of Single-Phase Flows in an Advanced-Flow Reactor », *Ind. Eng. Chem. Res.*, vol. 54, nº 30, p. 7543-7553, 2015, doi: 10.1021/acs.iecr.5b00232.
[12] E. V. Rebrov, J. C. Schouten, et M. H. J. M. de Croon, « Single-phase fluid flow distribution and heat transfer in microstructured reactors », *Chem. Eng. Sci.*, vol. 66, nº 7, p. 1374-1393, 2011, doi: 10.1016/j.ces.2010.05.044.
[13] C. Fernández-Maza, M. Fallanza, L. Gómez-Coma, et I. Ortiz, « Performance of continuous-flow micro-reactors with curved geometries. Experimental and numerical analysis », *Chem. Eng. J.*, vol. 437, nº January, Art. nº January, 2022, doi: 10.1016/j.cej.2022.135192.
[14] S. Hapke, G. A. Luinstra, et K. M. Zentel, « Optimization of a 3D-printed tubular reactor for free radical polymerization by CFD », *J. Flow Chem.*, p. 1-14, 2021.
[15] M. J. Nieves-Remacha, A. A. Kulkarni, et K. F. Jensen, « Hydrodynamics of liquid–liquid dispersion in an advanced-flow reactor », *Ind. Eng. Chem. Res.*, vol. 51, nº 50, p. 16251-16262, 2012.
[16] V. Viktorov, M. R. Mahmud, et C. Visconte, « Numerical study of fluid mixing at different inlet flow-rate ratios in Tear-drop and Chain micromixers compared to a new HC passive micromixer », *Eng. Appl. Comput. Fluid Mech.*, vol. 10, nº 1, p. 182-192, 2016.
[17] C. Parra-Cabrera, C. Achille, S. Kuhn, et R. Ameloot, « 3D printing in chemical engineering and catalytic technology: structured catalysts, mixers and reactors », *Chem. Soc. Rev.*, vol. 47, nº 1, p. 209-230, 2018.
[18] Y. Chen et P. Cheng, « Heat transfer and pressure drop in fractal tree-like microchannel nets », *Int. J. Heat Mass Transf.*, vol. 45, nº 13, p. 2643-2648, 2002.
[19] P. R. Gunjal et V. V. Ranade, « Modeling of laboratory and commercial scale hydro-processing reactors using CFD », *Chem. Eng. Sci.*, vol. 62, nº 18-20, p. 5512-5526, 2007.
[20] Z. Ni, E. Seebauer, et R. I. Masel, « Effects of microreactor geometry on performance: differences between posted reactors and channel reactors », *Ind. Eng. Chem. Res.*, vol. 44, nº 12, p. 4267-4271, 2005.
[21] M. Pan, Y. Tang, L. Pan, et L. Lu, « Optimal design of complex manifold geometries for uniform flow distribution between microchannels », *Chem. Eng. J.*, vol. 137, nº 2, p. 339-346, 2008.
[22] A. P. Sasmito, J. C. Kurnia, et A. S. Mujumdar, « Numerical evaluation of transport phenomena in a T-junction microreactor with coils of different configurations », *Ind. Eng. Chem. Res.*, vol. 51, nº 4, p. 1970-1980, 2012.
[23] A. Hamdache et M. Belkacem, « Effects of a zero normal-concentration-gradient outflow boundary condition on concentration polarization in a CFD study of a reverse osmosis process », *J. Braz. Soc. Mech. Sci. Eng.*, vol. 40, nº 11, Art. nº 11, 2018.
[24] T. Frey *et al.*, « CFD analysis of asymmetric mixing at different inlet configurations of a split-and-recombine micro mixer », *J. Flow Chem.*, vol. 11, nº 3, Art. nº 3, 2021, doi: 10.1007/s41981-021-00178-x.